

Cite this: DOI: 00.0000/xxxxxxxxxx

Solvent-Aware 2D NMR Prediction via Multi-Tasking Pre-Training and Iterative Unsupervised Learning[†]

Yunrui Li,^{‡a} Hao Xu,^{‡a} and Pengyu Hong^{*a}Received Date
Accepted Date

DOI: 00.0000/xxxxxxxxxx

Nuclear magnetic resonance (NMR) spectroscopy is crucial across diverse scientific fields, revealing detailed structural information, electronic properties, and molecular dynamic insights. Accurate prediction of NMR peaks in a spectrum from molecular structures allows chemists to effectively evaluate candidate structures by comparing predictions with actual shifts in experimental NMR spectra. This process facilitates peak assignments, thereby aiding in verifying molecular structures or identifying discrepancies. Although significant progress has been made in predicting one-dimensional (1D) NMR with Machine Learning (ML) approaches, 2D NMR prediction remains a challenge due to the lack of an annotated 2D NMR training dataset. To address this gap, we propose an Iterative Unsupervised Learning (IUL) approach to train a machine learning model for predicting atomic 2D NMR cross peaks and annotating peaks in experimental 2D NMR spectra. Initially, the model undergoes a Multi-Task pre-Training (MTT) phase using a set of annotated 1D ¹H and ¹³C NMR spectra. Then, the model is iteratively improved through a fine-tuning process with IUL, alternating between using the model to annotate the unlabeled 2D NMR data and refining the model using the newly generated annotations. Using the proposed approach, we trained our model on 19,000 Heteronuclear Single Quantum Coherence (HSQC) spectra, tested it on 500 HSQC spectra with expert annotations, and further compared it with two traditional methods (*ChemDraw* and *Mestrenova*) on another expert-annotated HSQC dataset. For HSQC cross peak prediction, our model achieves Mean Absolute Error (MAE) of 2.035 ppm and 0.163 ppm for ¹³C shifts and ¹H shifts on the test dataset, respectively, and outperforms the conventional tools. This performance demonstrates not only the model's capability in accurately predicting chemical shifts, but also its effectiveness in peak assignments for experimental HSQC spectra.

1 Introduction

Nuclear magnetic resonance (NMR) spectroscopy has emerged as a versatile tool with widespread applications across diverse scientific domains, including chemistry, environmental science, food science, material science, and drug discovery by unraveling molecular dynamics and structures.¹⁻³ The primary information of an NMR spectrum arises from the chemical shift, which is determined by the local environment of a nucleus and influenced by interactions through chemical bonds and space. This mechanism yields unique “fingerprints” corresponding to diverse functional groups or molecular motifs, thereby facilitating the streamlined deduction of atomic connectivity and arrangement.

Interpreting NMR spectra requires following essential guidelines, often referred to as “rules of thumb”, where specific chemical shifts are associated with distinctive functional groups.⁴

The determination of molecular structures from varying chemical shifts on NMR spectra generally requires the expertise of experienced organic chemists. To facilitate the interpretation of NMR spectra, significant efforts have been directed towards computational simulation of NMR spectra.⁵ Early computational approaches, like the Hierarchically Ordered Spherical Environment (HOSE) codes⁶, aim to encapsulate atom neighborhoods in concentric spheres, utilizing a nearest-neighbor approach to predict NMR shift values. A recent HOSE approach⁷ yields mean absolute errors (MAEs) of 3.52 ppm for ¹³C NMR and 0.29 ppm for ¹H NMR on the nmrshiftdb2⁸ dataset. Concurrently, significant efforts have been devoted to the ab initio calculation of NMR properties.^{9,10} Density Functional Theory (DFT)-based methods were developed for certain small organic molecules, achieving MAEs of 2.9 ppm for ¹³C NMR and 0.23 ppm for ¹H NMR.¹¹ However, the accuracy of these DFT-based methods relies heavily on the choice of the basis functions, which often require meticulous case-by-case manual tuning for each molecule. Moreover, the time-intensive nature of DFT calculations limits their applications to comprehensive and large datasets. Recently, the rise

^a Department of Computer Science, Brandeis University, USA; E-mail: hong-peng@brandeis.edu

[‡] These authors contributed equally to this work.

of Graph Neural Networks (GNN) and their successes in predicting molecular properties^{12–16} has prompted initiatives to employ GNNs for predicting peaks in NMR spectra. The application of GNN to molecules is intuitive, as a molecular structure can be naturally represented as a graph, with each atom as a node and its chemical bonds as edges. On 1D NMR data, a GNN-based model achieves MAEs of 1.355 ppm for ¹³C NMR and 0.224 ppm for ¹H NMR on the nmrshiftdb2 dataset.¹⁷ While considerable efforts have been made in developing predictive models for 1D NMR, the prediction of 2D NMR remains underexplored.

Heteronuclear Single Quantum Coherence (HSQC) spectroscopy¹⁸, a sophisticated 2D NMR technique, serves as a pivotal tool for elucidating atomic connectivity within complex molecules where conventional 1D NMR may prove insufficient.^{19,20} By correlating the chemical shifts of hydrogen nuclei with those of heteronuclear nuclei, typically carbon or nitrogen, via scalar coupling interactions, HSQC facilitates the comprehensive mapping of interatomic connections within a molecule. This mapping yields crucial insights into chemical bonding, molecular conformation, and intramolecular interactions. A notable stride in this domain utilizes the ML approach to establish correlations between DFT-simulated HSQC spectra and empirical data to identify molecules.²¹ However, the accurate prediction of HSQC spectra using ML techniques remains elusive. These obstacles primarily arise from the following factors: the scarcity of annotated datasets for training ML models, difficulties in handling the inherent sparsity of HSQC spectra which complicates feature representation, the computational demands required for accurate full-spectrum prediction, and the need for an in-depth comprehension of molecular structures.

In light of the aforementioned challenges and opportunities in interpreting HSQC spectra, we propose a novel solvent-aware machine learning model designed to predict HSQC cross peaks based on molecular structures, with the capability of peak assignment for experimental spectra, illustrated in Figure 1. Alongside a Graph Neural Network (GNN) module capturing structural nuances, the model incorporates a solvent encoder to effectively account for the impact of solvent environments on chemical shifts, which is essential for delivering accurate cross peak prediction and peak assignment of HSQC spectra. To tackle the lack of annotated HSQC data, we designed a two-step training process. First, the model is pre-trained on a labeled 1D NMR dataset via Multi-Task pre-Training (MTT), enabling it to learn a wide range of C–H interactions. Then, we implement the Iterative Unsupervised Learning (IUL) strategy that uses the unlabeled HSQC dataset to refine the model’s ability to accurately discern and label HSQC cross peaks. The model is thoroughly evaluated and compared to traditional tools like *ChemDraw*²² and *Mestrenova*²³ using expert-annotated test datasets. It demonstrates superior accuracy across all molecular weight categories compared to these traditional tools.

2 Methods

In this section, we explain the components of our model and the training strategy in detail.

2.1 2D NMR prediction model

As illustrated in Figure 1(A), our model contains a GNN component for encoding molecular features and a solvent encoder component for embedding solvent information. The GNN component learns atomic embeddings that capture both the local and global chemical environments of each atom, which are essential for understanding the observed NMR chemical shifts. The learnt atom representations are expanded by the solvent embedding, and then are mapped to ¹³C and ¹H cross peaks by a multilayer perceptron (MLP) component.

2.1.1 GNN

A molecule can be represented by a graph $G = (V, E)$, where V is the node set representing atoms and E is the edge set representing chemical bonds. Three features are provided for each node: atomic type, chirality, and hybridization. Also, two features are considered for each edge: bond type and bond direction. Bond types include Single, Double, Triple, and Aromatic, each reflecting a distinct configuration of electron sharing between atoms. Bond direction includes None, EndUpRight, and EndDownRight, primarily representing stereochemistry in double bonds. Each atom’s feature vector is embedded into a representation vector by a learnable encoder. Similarly, each edge’s feature vector is embedded into a representation vector of the same length by another learnable encoder. Then, a GNN model^{24–28} utilizes the message passing mechanism to iteratively refine the representation of each node based on information from its neighbors and connected edges. This mechanism allows the learnt node representation to effectively capture structural context, reflecting the foundational principles of atomic interactions. Our implementation of the message passing mechanism is illustrated in 2. It iterates for a predefined number of layers L , facilitating the propagation of information throughout the graph. Consequently, each node can gradually accumulate information from a wider neighborhood across successive layers. This allows the final representation of each node to capture both local and global structural information. Our model features 5 GNN layers, with an atomic embedding dimension of 512.

2.1.2 Solvent encoder

Since the solvent has a profound impact on NMR chemical shifts, we incorporated a trainable solvent encoder component into our model to accurately capture this influence. We identified the following 9 principal solvent groups based on their prevalence in our dataset and domain-specific understandings of their distinct impacts on NMR shifts. These groups include trichloromethane, dimethyl sulfoxide, acetone, acids, benzene, methanol, pyridine, water, and an additional category to encompass any unspecified solvents from our dataset (termed "unknown"). The solvent encoder transforms each discrete solvent group i into a unique, dense feature vector S_i^d , where d is the embedding dimension. These learnable vectors are optimized alongside other model parameters during training, resulting in representations that accurately reflect the impact of each solvent class. Given the different sensitivities of carbon (C) and hydrogen (H) nuclei to solvent environments, we choose different embedding dimension d to tailor

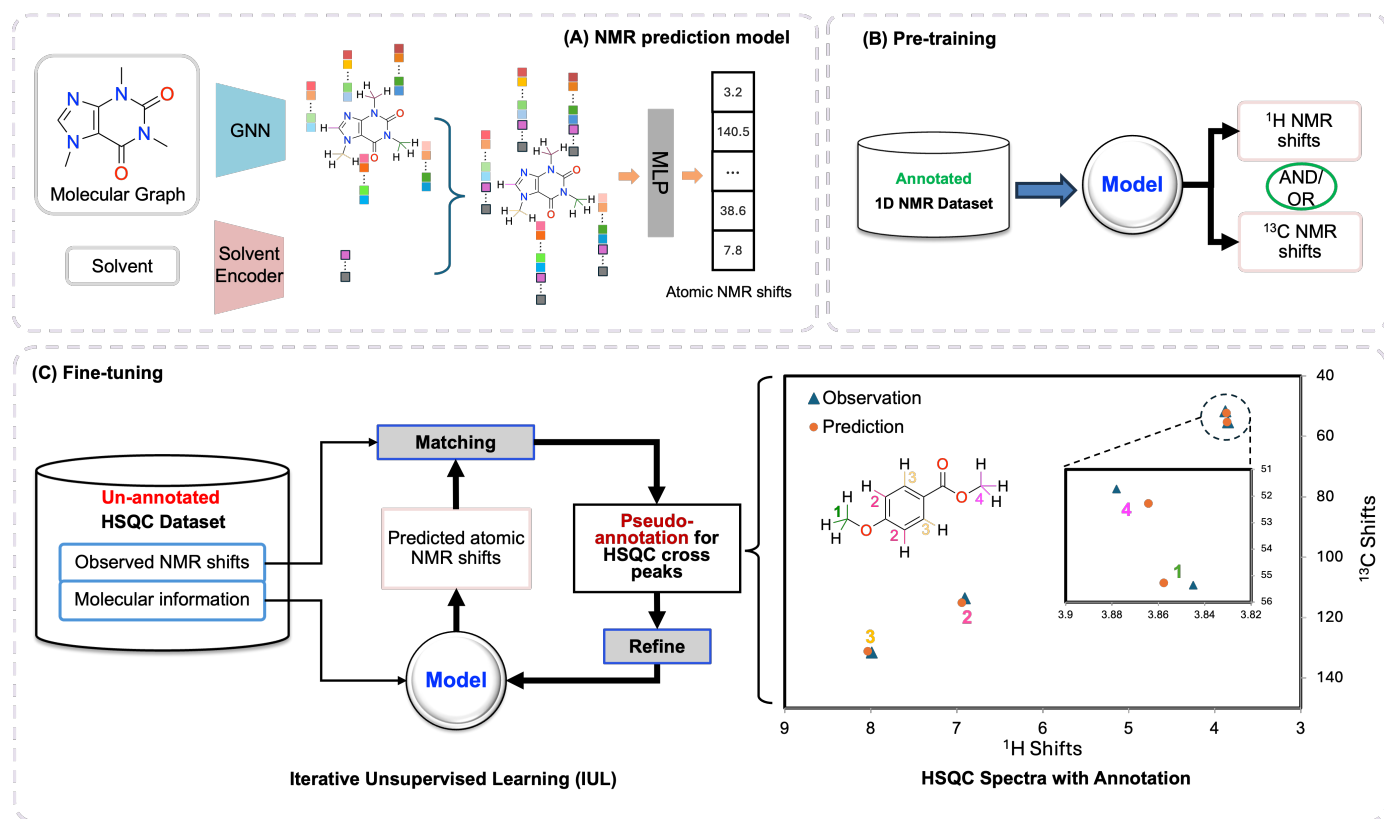


Fig. 1 Illustration of model design (A) and training strategy ((B) and (C)). (A) The model takes a molecular structure and derives its atomic representations by a GNN. The solvent information is encoded into a latent representation via the Solvent encoder. The representation of each atom is concatenated with the solvent representation, which is then used to predict the atomic NMR shifts using an MLP component. The cross peak predictions are generated by linking the atomic predictions based on their connectivity in the molecular graph. (B) Model pre-training on the annotated 1D NMR dataset using MTT. (C) The pre-trained model is refined through the IUL process using the unlabeled HSQC dataset. The final output of the model has both the HSQC cross peaks and atom alignment.

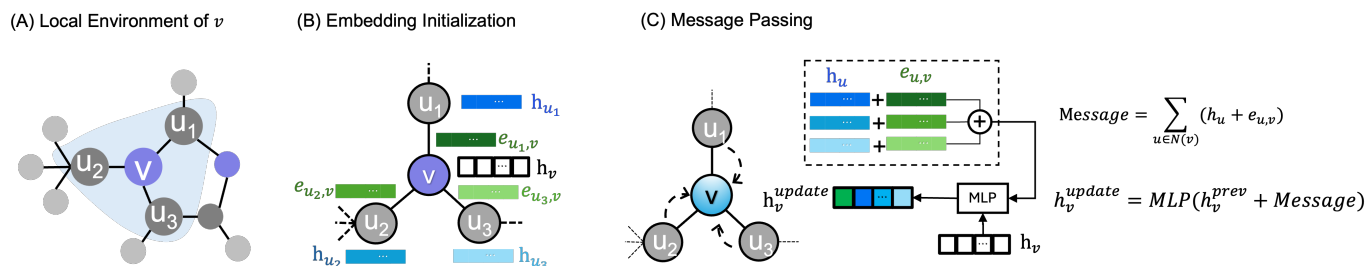


Fig. 2 Illustration of message passing and node representation updates in a GNN layer. (A) For a given center atom in a molecular graph, the local environment contains the neighborhood atom that is directly bonded to the center atom. (B) For a center node (v), initial random representations are assigned to this node, its neighboring nodes (u_1, u_2, u_3), and their connecting bonds ($e_{u_1,v}, e_{u_2,v}, e_{u_3,v}$). (C) Message Passing and node update. Representations of all neighboring nodes and edges are aggregated and integrated to form a message to the center node. The representation of the center node is then updated to incorporate this message and information from its previous state.

the solvent effect modeling for each nuclei type. A larger embedding dimension d allows the embedding to more effectively capturing the nuanced influence of solvents on NMR shifts. In our implementation, the solvent embedding dimension is 32.

2.1.3 Atomic NMR shift prediction

Finally, the embedding of each atom $h_v^{(L)}$ and the solvent embedding S_i^d for each solvent class i are concatenated to produce a holistic representation of the atom within the context of its molecular structure and the given solvent. This combined representa-

tion is subsequently processed by a MLP network to predict the NMR shifts for the atom:

$$y_v = \text{MLP}(h_v^{(L)} \oplus S_i^d) \quad (1)$$

where y_v is the predicted chemical shift of atom v , $h_v^{(L)}$ is the atom level embedding produced by GNN, S^d is the solvent embedding, and \oplus is the concatenation operation. By integrating solvent embedding and atomic embedding, the model effectively combines intrinsic molecular properties and solvent effects, en-

hancing its ability to predict atomic NMR shifts accurately.

Two separate MLP modules are used for predicting ^{13}C and ^1H shift in the cross peak predictions, respectively. Each C atom can bond up to 4 H atoms. When bonded to one, three, or four H atoms, a C atom typically shows only one cross peak in an experimental spectrum. However, when a C atom is connected to two H atoms, up to two cross peaks may be observed, depending on the chiral center. Consequently, a C atom can exhibit at most two ^{13}C and ^1H cross peaks. In light of this observation, one MLP module is dedicated to predicting the ^{13}C shifts and another MLP module for the corresponding ^1H shifts. For cross peak predictions, the ^{13}C shifts are predicted using the embeddings of C atoms. The corresponding ^1H shift predictions for each C atom incorporate aggregates of embeddings from all bonded H atoms, resulting in two predictions that are typically very similar when only one cross peak is theoretically possible. This design enhances the model's accuracy in predicting ^1H shifts by leveraging the C atom-centered aggregation of the H atom context. By integrating the contextual dynamics around each C atom, the model provides a more detailed and accurate mapping of hydrogen environments, crucial for pinpointing precise cross peaks in complex HSQC spectra. In our implementation, we used 2 MLP layers, with the hidden dimensions to be 128 and 64 respectively.

2.2 Training strategy

The cross peaks are notably sparse in an HSQC spectrum, where typical resolutions for ^{13}C and ^1H shifts are 0.1 and 0.01 ppm, respectively. A typical HSQC spectrum can include 20,000 readings, covering ^{13}C shifts from 0 to 200 ppm and ^1H shifts from 0 to 10 ppm. However, almost all of these readings are zeros, with only a small fraction representing the potential cross peaks of C–H bonds, crucial for molecular structure analysis. Moreover, the scarcity of annotated HSQC data, particularly the labor-intensive annotations that link cross peaks to C–H bonds, makes model training difficult. To deal with this issue, we deployed MTT to pre-train the model using an extensive annotated 1D NMR dataset (Fig. 1B). This step acclimates the model with a broad range of molecular structures and their chemical shifts, and enables it to capture the intricate interplay between molecular structures and their NMR characteristics. Subsequently, we utilize the IUL strategy to refine the model further on the HSQC dataset (Fig. 1C). Through iterative cycles of prediction, annotation, and re-training, the model progressively enhances its understanding of the complex relationships and patterns within the HSQC spectra, thus improving its predictive accuracy and providing precise cross peak alignments. By combining the MTT and IUL, we extend our annotation capabilities from 1D to 2D data, thereby enhancing the model's predictive power and utility as a robust tool for NMR spectra analysis.

2.2.1 Pre-training on 1D NMR data

In the pre-training phase, we utilized approximately 24,000 annotated 1D NMR data points. Among these, around 22,000 samples exclusively feature ^{13}C shifts, approximately 400 samples solely exhibit ^1H shifts, while roughly 1,600 samples contain both ^1H and ^{13}C shifts. To train the model effectively for predicting both

^1H and ^{13}C shifts, we adapt the MTT approach, which enables simultaneous training on multiple related tasks. When the input data contains ^{13}C shifts, the model predicts only carbon shifts and assesses the errors between the predicted and actual values. Conversely, when the data sample contains ^1H shifts, the hydrogen shift prediction module is activated. In both scenarios, the embeddings of ^{13}C and ^1H atoms in the GNN module are updated simultaneously, benefiting from the message passing mechanism. Therefore, the learnt representations implicitly contain a basic understanding of C–H relationships, essential for the interpretation of HSQC data. However, the relative scarcity of ^1H shift data, due to the difficulties in accurately obtaining and extracting peaks ^1H from experimental data, complicates the training process as focusing extensively on one type of shift could compromise the model's ability to accurately predict the other. To handle this problem in the MTT training, we performed over-sampling on a subset of data that contain both ^1H and ^{13}C shifts, and those containing only ^1H shifts. Consequently, the learned representations develop a fundamental understanding of C–H relationships, crucial for interpreting HSQC data effectively. This integration of learned atomic relationships streamlines the transition to HSQC cross peak predictions, thereby enhancing the model's accuracy and efficiency in analyzing HSQC spectra.

2.2.2 Unsupervised fine-tuning on HSQC data

The model pre-trained on the 1D NMR dataset has limited ability to predict HSQC cross-peaks from molecular structures. The reason is two-fold. First, there is a substantial difference between the nature of 1D NMR data and HSQC data. The chemical shifts observed in HSQC cross peaks often do not correlate directly with their counterparts in 1D NMR spectra, particularly regarding ^1H shifts. For example, in the 1D NMR data, the chemical shifts of non-singlet peaks are averaged as ground truth, lacking the precision required by HSQC. Also, the variations in relaxation properties, coupling effects, and fluctuations in the local magnetic field can all contribute to the distinctions between 1D NMR and HSQC peaks. Moreover, experimental conditions and pulse sequences used in HSQC experiments can introduce slight deviations in chemical shift values compared to those observed in the ^1H spectrum. Second, the molecule distributions in our 1D NMR data and HSQC data exhibit significant differences. The HSQC dataset comprises 76.34% small molecules and 90.33% non-saccharides, whereas the 1D NMR dataset contains 98.80% small molecules and 99.95% non-saccharides.

Therefore, it is necessary to refine the pre-trained NMR prediction model on the HSQC dataset. However, the HSQC dataset is not annotated. In response, we implement an IUL training strategy (Fig. 1C), which iterates between (a) aligning cross peak prediction from the model with the experiment observations to annotate the HSQC data and (b) using the newly acquired annotations to fine-tune the NMR prediction model, until convergence.

2.2.3 Pseudo-annotation of HSQC

At the end of each round in the IUL process, the model's predicted signals are aligned with the experimental observations to create pseudo-labels. In straightforward cases where the number

of C–H bonds in a molecular graph matches the observed HSQC cross peaks, the Hungarian algorithm^{29,30} is used. This classic optimization technique solves assignment problems by minimizing the cost of matching a set of predictions to a set of observations. In the context of NMR analysis, the “cost” is defined as the discrepancy between the predicted chemical shifts and the actual shifts observed experimentally. By systematically reducing these differences, the Hungarian algorithm achieves an optimal one-to-one correspondence between predicted shift pairs and experimental signals, even in complex scenarios with potential signal overlap.

However, in most cases, the number of C–H bonds within a molecule exceeds the number of signals recorded, making peak alignment more difficult. This mismatch in numbers arises from several factors: firstly, rotational equivalence can reduce the number of signals, with a single peak representing all three C–H bonds for methyl groups; secondly, symmetrical molecular structures can result in a single detectable signal for multiple symmetric C–H bonds, as seen in benzene molecule where only one peak represents all six C–H bonds; lastly, in highly complex molecules, overlapping signals obscure some peaks, reducing the detectability of individual C–H bonds from experiments.

To overcome this issue, we utilize the graduated assignment algorithm^{15,31}, which facilitates matching between graphs of different node counts, making it particularly suitable for this scenario. In this algorithm, our model’s predicted C–H shifts $(C^i, H^i)_{i=0}^N$ and the observed C–H signals $(C^j, H^j)_{j=0}^M$ of each molecule are conceptualized as points on a 2D plane, where N and M are numbers of predicted and observed C–H shifts respectively. These points are then treated as vertices in two fully connected graphs, G_1 for predicted shifts and G_2 for observed signals. The similarity between nodes is defined as the inverse of differences between predicted chemical shifts (node in G_1) and observed shifts (node in G_2). Specifically, for each predicted shift, we compute its difference with every observed shift, where a smaller difference indicates a higher similarity. We derive the assignment matrix A where each element $A_{uv} \in \{0, 1\}$ indicates whether node u in G_1 matches with node v in G_2 , the algorithm first finds the soft matching matrix that relaxes the binary constraint $A_{uv} \in \{0, 1\}$ to a continuous range $[0, 1]$, then converts it into hard assignment in a greedy way, enabling one-to-many matching.

3 Results

3.1 Data

The pre-training dataset used in the MTT process is a 1D NMR dataset from NMRShiftDB²⁸, which contains $\sim 24,000$ annotated NMR spectra collected from 22,663 distinct molecules. The datasets used in the IUL process consist of a training dataset containing $\sim 19,000$ experimental HSQC spectra and a validation dataset containing $\sim 5,000$ HSQC spectra, collected from HMDB³² and CH-NMR-NP³³. To quantitatively evaluate our model, we built a test dataset by randomly selecting 500 spectra and manually annotating them to establish the ground truth. These 500 spectra were randomly divided into 5 subsets of 100 spectra each, allowing us to conduct the assessment 5 times and

evaluate the variation in performance. This test dataset was used to produce the results presented in Section 3.2, 3.4, 3.5, and 3.6. Additionally, to compare our model with two conventional tools (ChemDraw and Mestrenova) in chemistry, we created the second test dataset by randomly selecting a set of molecules and manually annotating their HSQC spectra to obtain 150 cross-peaks. The comparison results are presented in Section 3.3. The second test dataset is relatively small as it is labor-intensive to derive HSQC shifts from molecular formulas using these established tools. To ensure the coverage of the second test set, when selecting the molecules, we stratified all candidates into three weight groups (0-499 Dalton, 500-999 Dalton, and 1000+ Dalton) and randomly selected molecules from each weight group, resulting in 50 annotated cross peaks per groups.

3.2 Performance on HSQC cross peak prediction and assignment

Table 1 summarizes the performance of our model on the tasks of HSQC cross peak prediction and peak assignment using the 1st test dataset. Specifically, the model achieved an MAE of 2.06 ppm for ^{13}C shifts and 0.16 ppm for ^1H shifts. The robustness of our approach results in exceptionally high accuracy for peak assignments at both the molecular and peak levels, achieving 98.6% and 99.79% respectively. Our model is said to be correct on a molecule if all cross peaks of the molecule are correctly assigned. The peak level accuracy is calculated as the ratio of correctly assigned cross peaks to the total number of cross peaks. Figure 3 illustrates an example of the model outcome of peak prediction and assignment, using inputs of molecule and solvent.

Table 1 Performance on HSQC cross peak prediction and peak assignment for the 1st test set. This table reports the Mean Absolute Error (MAE) and the accuracy of peak assignments (the pseudo annotations) produced by our approach. The numbers in the parentheses are the standard deviations.

MAE (ppm)		Peak Assignment Accuracy (%)	
^{13}C Shift	^1H Shift	Molecule	Peaks
2.035 (0.088)	0.163 (0.003)	98.6 (0.55)	99.79 (0.12)

3.3 Comparison with traditional tools

In organic chemistry, simulating HSQC spectra is crucial for analyzing experimental HSQC spectra, as it assists researchers in assigning the observed cross peaks to the C–H bonds in target molecules. Traditional approaches, including software solutions such as ChemDraw²², and Mestrenova²³, have long served as the primary resources for this task. We compared our model with ChemDraw and Mestrenova on the second test dataset. The results (see Table 2) clearly demonstrate the superiority of our model. Figure 4 illustrates two examples with different molecular sizes, showing the advantage of our model.

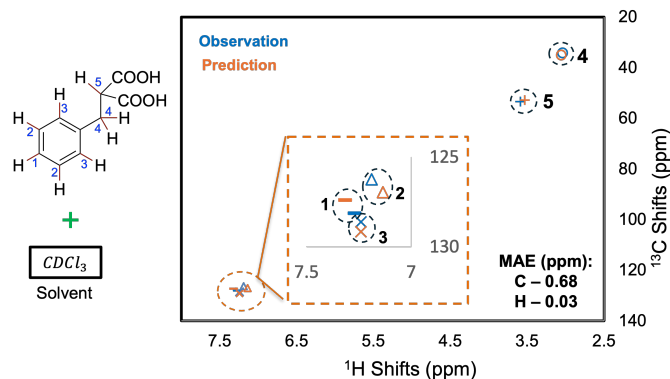


Fig. 3 An example of using our model to accurately predict cross peaks and align them with experimental signals. The molecule is shown at the top-left, where each C–H bond is labeled with a numerical identifier. Notably, the symmetric pairs of bonds (labeled as “2”, “3”, and “4”) are each expected to generate a single HSQC cross peak due to their structural equivalence. The HSQC cross peaks predicted by our model (in orange) and their alignments to the experimental observations (in blue) are plotted in the right. The alignments are indicated by the dash circles.

Molecular Weight	ML Model MAE		ChemDraw MAE		Mestrenova MAE	
	¹³ C	¹ H	¹³ C	¹ H	¹³ C	¹ H
0 - 499	1.128	0.095	1.391	0.292	1.293	0.141
500 - 999	1.031	0.091	2.362	0.215	1.699	0.112
1000+	3.891	0.171	6.862	0.601	7.748	0.409
Overall	2.003	0.119	3.529	0.367	3.559	0.219

Table 2 Performance comparison between our proposed model and established traditional tools on the second test dataset. Our model performs better across all molecular weight categories.

3.4 Performance by molecular weights

Molecular weight is a general indicator of a molecule’s complexity, encompassing varied geometries, bonding patterns, and the presence of isomers. These factors contribute to increased intramolecular interactions, resulting in spectral complexity such as closely spaced peaks or overlapping signals. Additionally, the increased number of spin-spin interactions within larger molecules necessitates more advanced NMR techniques to achieve sufficient resolution.³⁴ Furthermore, solubility issues can lead to weak signals, further complicating spectral analysis. Consequently, interpreting HSQC spectra for medium and large molecules is challenging. Therefore, there is a pressing need for a model that can effectively predict and analyze HSQC spectra for these complex molecules.

To address this challenge, we evaluated the robustness of our model on 1st test dataset comprising complex medium and large molecules, testing its performance across a range of molecular weights. The results are stratified by molecular weights (MW) in Figure 5. The test molecules are grouped into three categories: small (MW < 500 daltons), medium (500 ≤ MW < 1000 daltons), and large (1000 daltons ≤ MW). On the task of predicting ¹H shifts of HSQC cross peaks, the model performs comparably across all groups, achieving excellent MAEs of 0.16 - 0.17 ppm. On the task of predicting ¹³C shifts, the model achieves an MAE of 1.91 ppm for medium-sized molecules. Our model

demonstrates a good generalization power on large molecules and achieves a MAE of 2.14ppm on predicting ¹³C shifts for this category, despite the training data containing only a small proportion of large molecules (~2%).

3.5 Performance on saccharides

Saccharides, or carbohydrates, play critical roles in various biological processes involved in energy source and storage, cell signaling, cell adhesion, cell recognition, structural integrity of cells and tissues, as well as cognitive functions and metabolic regulation.^{35–38} Despite their importance, elucidating the structures of saccharides is challenging due to their inherent structural complexity and diversity. This complexity arises from the diverse arrangements of monosaccharide units, varied anomeric configurations, and variable glycosidic linkages. Additionally, carbohydrates often lack the crystallinity required for high-resolution X-ray diffraction, unlike the well-defined crystalline structures of small molecules or proteins. Consequently, NMR spectroscopy, particularly through techniques such as HSQC, has emerged as an indispensable tool in unraveling the detailed structures of carbohydrates.^{39,40} Forecasting HSQC cross peaks and aligning them with experimental data can assist in comprehending saccharide connectivity and stereochemistry, thus aiding in structural determination.

Our model demonstrates excellent performance in predicting HSQC cross peaks for saccharides molecules, yielding an MAE of 1.95 for ¹³C shifts and 0.17 for ¹H shifts (see Figure 6). This level of accuracy, consistent with the overall model performance in Table 1, demonstrates the model’s robustness in handling complex saccharide structures. Figure 7 shows the performance of our model on a few exemplar saccharides. These saccharides feature multiple ring structures and numerous stereogenic centers, contributing to the intricate nature of their HSQC spectra. Despite these inherent complexities, our model exhibits exceptional accuracy in predicting the HSQC cross peaks for these molecules. This robust performance underscores our model’s capacity to navigate the complexities associated with saccharides, thereby emphasizing its versatility and effectiveness across various applications in the field.

3.6 Effects of pre-training and fine-tuning

Table 3 compares our model’s ability to predict HSQC cross peaks at different training stages, highlighting the contributions of our training strategy. After pre-trained via MTT on the 1D NMR dataset, the model achieved the validation performance with mean absolute errors (MAEs) of 0.210 ppm for ¹H NMR prediction and 2.228 ppm for ¹³C NMR prediction. This success can be attributed to MTT which allows the model to effectively learn atomic latent features as well as local structural information by simultaneously performing ¹H and ¹³C NMR shift predictions. This helps us surpass the problem with limited annotated HSQC data. Interestingly, the pre-trained model was able to predict HSQC cross peaks with reasonable MAEs of 1.397 ppm and 2.822 ppm for ¹H and ¹³C shifts, respectively. These relatively large MAEs are expected as the data distribution of the HSQC

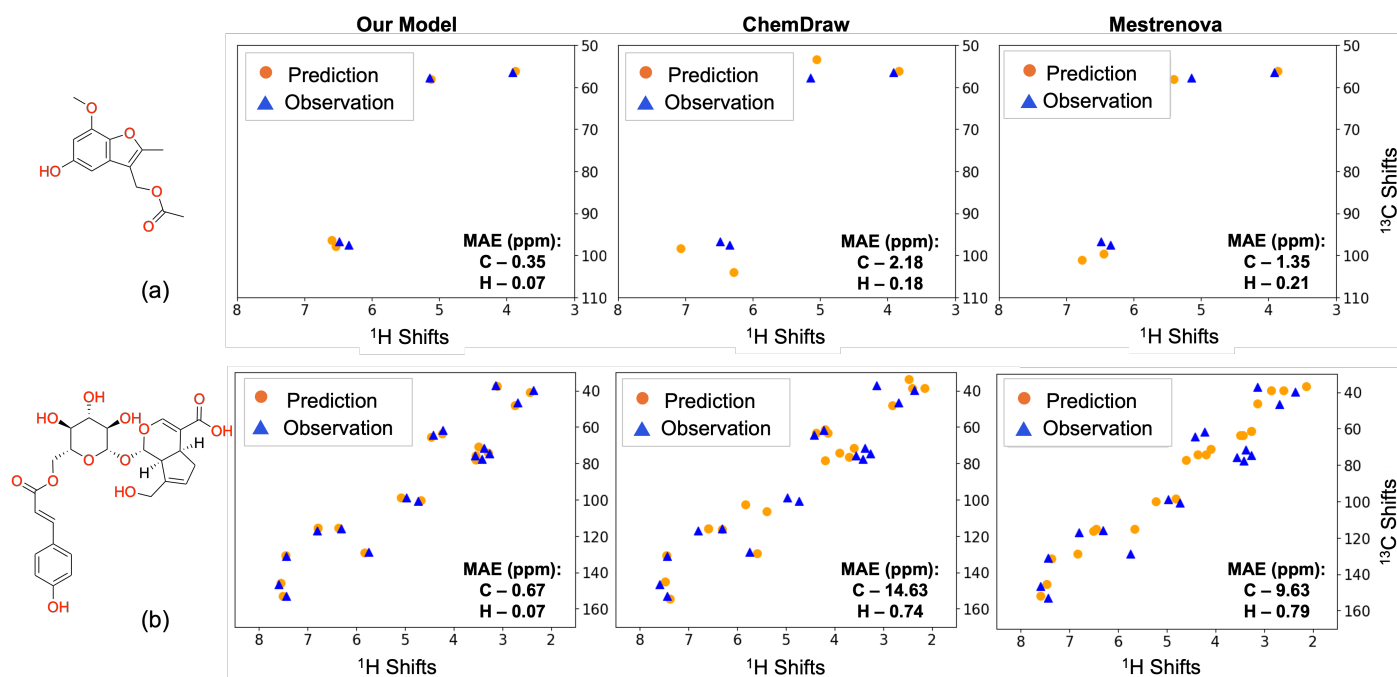


Fig. 4 Comparing our model, ChemDraw, and Mestrenova on two typical examples. A small molecule (a) with weight of ~ 250 Dalton and a larger molecule (b) with weight of ~ 500 Dalton. The observed experimental signals and the predicted signals are colored in blue and orange, respectively. The prediction error (MAE) is shown in the bottom right corner of each plot. Our model performs better than ChemDraw and Mestrenova, and particularly excels in handling large molecules with complex conformations.

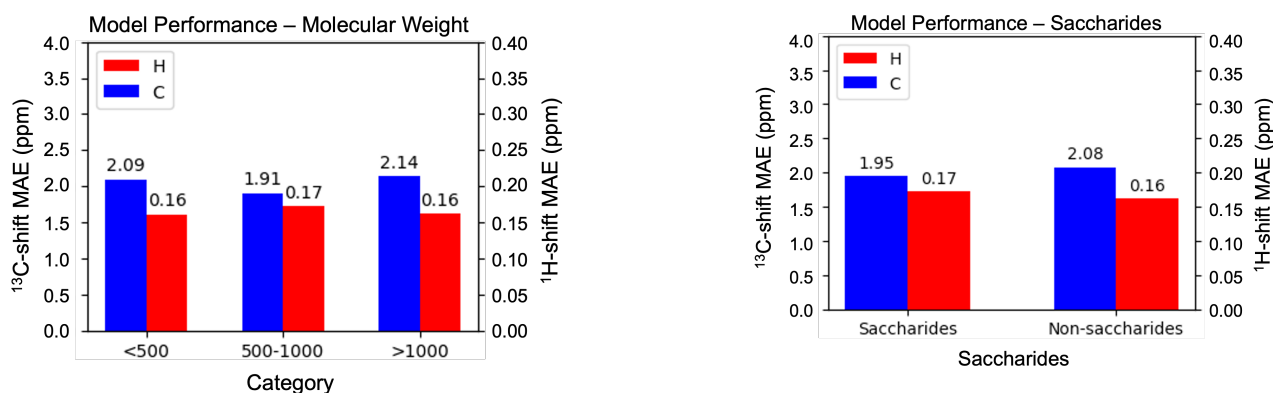


Fig. 5 Model performance comparison between small, medium, and large molecules by molecular weight. The model performs equally well between small and medium molecules, with a marginally reduced precision for larger molecules.

dataset (76.34% small molecules and 90.33% non-saccharides) differs significantly from that of the 1D NMR dataset (98.80% small molecules and 99.95% non-saccharides). In addition, the HSQC cross peaks involve interactions beyond simple pairings of 1D ^{13}C and ^1H shifts, requiring a deeper understanding of interactions between atoms. Finally, the frequent absence of solvent labels in the 1D NMR dataset prevents the model from learning solvent effects.

Nevertheless, the pre-training via MTT offers a robust foundation for fine-tuning the model using IUL. With each IUL iteration, we observed a reduction in model errors. The performance im-

Fig. 6 Model performance comparison between saccharides and non-saccharides. The model performs equally well in both groups.

provement is more pronounced during the initial iterations and gradually diminishes. By the fifth iteration, the improvement became marginal, indicating the convergence of fine-tuning. Finally, the fine-tuned model achieves MAEs of 0.163 ppm and 2.035 ppm for ^1H and ^{13}C shifts, respectively. Throughout the IUL process, the model was trained to gain a more profound understanding of solvent effects and complex C-H interactions due to intricate

Table 3 MAEs for 2D NMR prediction at different stages of training

Training Stage	^1H MAEs (ppm)	^{13}C MAEs (ppm)
MTT	1.397 (0.085)	2.822 (0.092)
MTT+ IUL	0.163 (0.003)	2.035 (0.088)

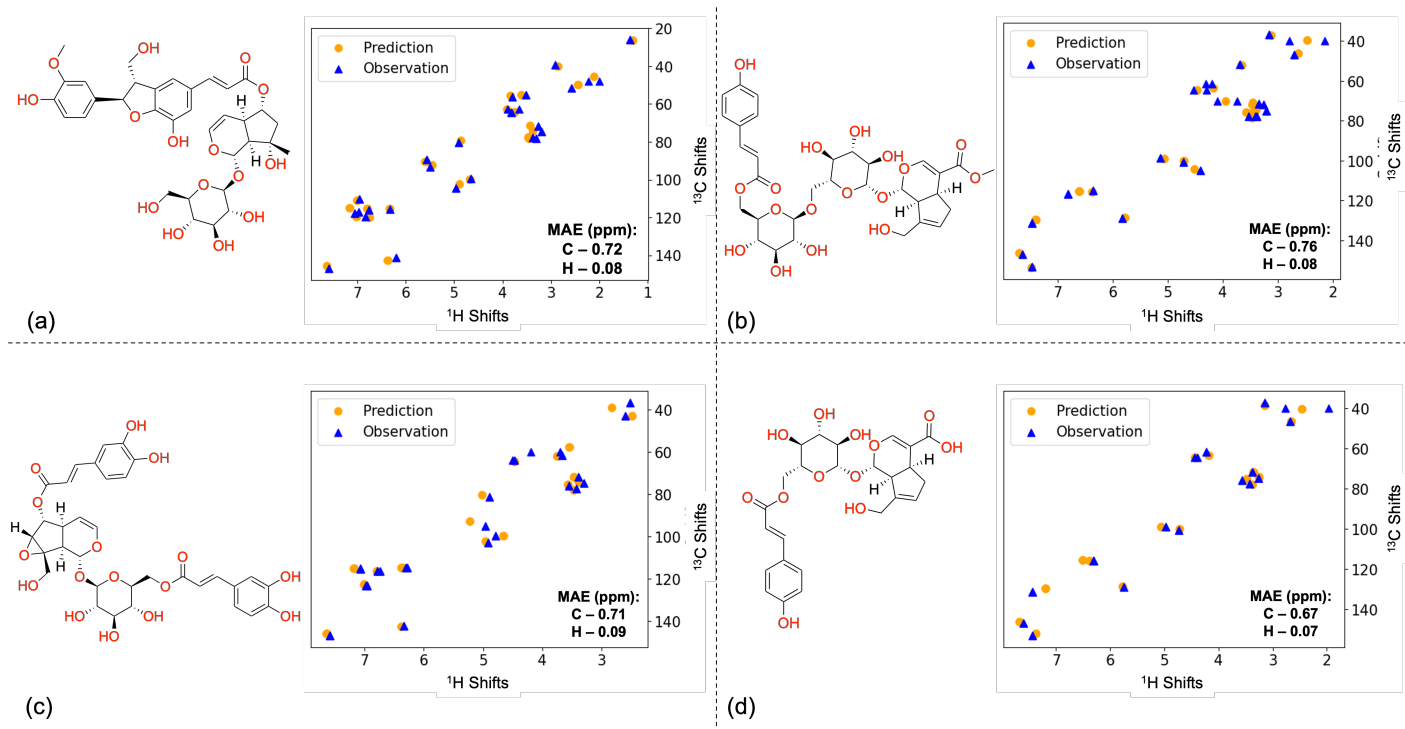


Fig. 7 Exemplary demonstration of our model's performance on saccharides. The observed experimental signals and the predicted signals are colored in blue and orange, respectively. The prediction error (MAE) is shown in the bottom right corner within each plot.

molecular structures.

4 Conclusions and Discussions

In this study, we introduce a novel framework to develop machine learning techniques for predicting C–H cross peaks in HSQC spectra. The framework enables us to tackle two major challenges in this avenue. The first challenge is the scarcity of annotated HSQC data for training machine learning models. The second challenge is that collecting large volumes of annotated HSQC data is labor-intensive and requires highly trained personnel. In implementing our framework, we developed a model combining a GNN with a solvent encoder. The GNN is trained to generate atomic embeddings that encapsulate both the local and global chemical environments of each atom, which is crucial for accurate chemical shift predictions. The atomic embeddings are combined with the solvent embedding produced by the solvent encode, which allows our model to learn the influence of solvent on chemical shifts. The combined embeddings are mapped by MLP modules to HSQC chemical shifts. Our framework employs a two-stage transductive strategy to train the model while addressing the aforementioned challenges. In the first stage, we use a large amount of annotated 1D NMR data to pre-train the model via Multi-Task learning. This enables the model to adeptly grasp the intricate relationship between atomic interactions and NMR signals, laying a robust foundation for the subsequent stage. Next, the model is refined on a set of unlabelled HSQC spectra via Iterative Unsupervised Learning, enhancing the model's capability in predicting and interpreting HSQC spectra. Our final model achieves MAEs of 0.163 ppm and 2.035 ppm for ^1H and ^{13}C shifts respectively, while ac-

curately assigning cross peaks. It demonstrates a consistent performance across various molecular weight and saccharide categories, significantly outperforming the traditional methods, and shows convincing generalization capabilities to less represented samples from the training dataset. In the future, we plan to refine our model by developing 3D-GNN models that are able to consider 3D structural information such as spatial orientation and conformational flexibility. This enhancement should enable us to handle other 2D NMR spectra, such as Correlation Spectroscopy and Nuclear Overhauser Effect Spectroscopy, thus broadening its applicability and making a more substantial contribution to the field of chemical analysis.

Data Availability

The codes will be made publicly available upon the date of publication, and the datasets will be available upon request.

Conflicts of interest

There are no conflicts of interest to declare.

Acknowledgements

This work was supported by GlycoMIP, a National Science Foundation (NSF) Materials Innovation Platform funded through Cooperative Agreement DMR-1933525, as well as NSF OAC 1920147.

Notes and references

- 1 H. Gunther and H. Gunther, *NMR spectroscopy: basic principles, concepts, and applications in chemistry*, John Wiley & Sons Chichester, UK, 1994.
- 2 T. D. Claridge, *High-resolution NMR techniques in organic chemistry*, Elsevier, 2016, vol. 27.
- 3 H.-Y. Yu, S. Myoung and S. Ahn, *Magnetochemistry*, 2021, **7**, 121.
- 4 E. Jonas and S. Kuhn, *Journal of cheminformatics*, 2019, **11**, 1–7.
- 5 E. Jonas, S. Kuhn and N. Schlörer, *Magnetic Resonance in Chemistry*, 2022, **60**, 1021–1031.
- 6 W. Bremser, *Analytica Chimica Acta*, 1978, **103**, 355–365.
- 7 S. Kuhn and S. R. Johnson, *ACS omega*, 2019, **4**, 7323–7329.
- 8 C. Steinbeck, S. Krause and S. Kuhn, *Journal of chemical information and computer sciences*, 2003, **43**, 1733–1739.
- 9 M. W. Lodewyk, M. R. Siebert and D. J. Tantillo, *Chemical Reviews*, 2012, **112**, 1839–1862.
- 10 P. H. Willoughby, M. J. Jansma and T. R. Hoye, *Nature protocols*, 2014, **9**, 643–660.
- 11 K. W. Wiitala, T. R. Hoye and C. J. Cramer, *Journal of Chemical Theory and Computation*, 2006, **2**, 1085–1092.
- 12 O. Wieder, S. Kohlbacher, M. Kuenemann, A. Garon, P. Ducrot, T. Seidel and T. Langer, *Drug Discovery Today: Technologies*, 2020, **37**, 1–12.
- 13 Z. Zhang, L. Chen, F. Zhong, D. Wang, J. Jiang, S. Zhang, H. Jiang, M. Zheng and X. Li, *Current Opinion in Structural Biology*, 2022, **73**, 102327.
- 14 X. Fang, L. Liu, J. Lei, D. He, S. Zhang, J. Zhou, F. Wang, H. Wu and H. Wang, *Nature Machine Intelligence*, 2022, **4**, 127–134.
- 15 Y. Wang, S. Chen, G. Chen, E. Shurberg, H. Liu and P. Hong, *Informatics*, 2023, p. 8.
- 16 H. Xu, Z. Zhou and P. Hong, *arXiv preprint arXiv:2401.17615*, 2024.
- 17 Y. Kwon, D. Lee, Y.-S. Choi, M. Kang and S. Kang, *Journal of chemical information and modeling*, 2020, **60**, 2024–2030.
- 18 G. Bodenhausen and D. J. Ruben, *Chemical Physics Letters*, 1980, **69**, 185–189.
- 19 N. Bross-Walch, T. Kühn, D. Moskau and O. Zerbe, *Chemistry & biodiversity*, 2005, **2**, 147–177.
- 20 Q. Li and C. Kang, *Molecules*, 2020, **25**, 2974.
- 21 M. M. Zanardi and A. M. Sarotti, *The Journal of organic chemistry*, 2015, **80**, 9371–9378.
- 22 N. Mills, *ChemDraw Ultra 10.0 CambridgeSoft*, 100 CambridgePark Drive, Cambridge, MA 02140. www.cambridgesoft.com. Commercial Price: 1910fordownload, 2150 for CD-ROM; Academic Price: 710fordownload, 800 for CD-ROM., 2006.
- 23 M. R. Willcott, *MestRe nova*, 2009.
- 24 F. Scarselli, M. Gori, A. C. Tsoi, M. Hagenbuchner and G. Monfardini, *IEEE transactions on neural networks*, 2008, **20**, 61–80.
- 25 A. Micheli, *IEEE Transactions on Neural Networks*, 2009, **20**, 498–511.
- 26 J. Gilmer, S. S. Schoenholz, P. F. Riley, O. Vinyals and G. E. Dahl, International conference on machine learning, 2017, pp. 1263–1272.
- 27 J. Zhou, G. Cui, S. Hu, Z. Zhang, C. Yang, Z. Liu, L. Wang, C. Li and M. Sun, *AI open*, 2020, **1**, 57–81.
- 28 P. Reiser, M. Neubert, A. Eberhard, L. Torresi, C. Zhou, C. Shao, H. Metni, C. van Hoesel, H. Schopmans, T. Sommer et al., *Communications Materials*, 2022, **3**, 93.
- 29 H. W. Kuhn, *Naval research logistics quarterly*, 1955, **2**, 83–97.
- 30 J. Munkres, *Journal of the society for industrial and applied mathematics*, 1957, **5**, 32–38.
- 31 S. Gold and A. Rangarajan, *IEEE Transactions on pattern analysis and machine intelligence*, 1996, **18**, 377–388.
- 32 D. S. Wishart, A. Guo, E. Oler, F. Wang, A. Anjum, H. Peters, R. Dizon, Z. Sayeeda, S. Tian, B. L. Lee et al., *Nucleic acids research*, 2022, **50**, D622–D631.
- 33 J-resonance, *NMR Database*, <https://www.j-resonance.com/en/nmrdb/>.
- 34 M. P. Foster, C. A. McElroy and C. D. Amero, *Biochemistry*, 2007, **46**, 331–340.
- 35 D. Guillén, S. Sánchez and R. Rodríguez-Sanoja, *Applied microbiology and biotechnology*, 2010, **85**, 1241–1249.
- 36 Y. Yu, M. Shen, Q. Song and J. Xie, *Carbohydrate polymers*, 2018, **183**, 91–101.
- 37 M. Dashty, *Clinical biochemistry*, 2013, **46**, 1339–1352.
- 38 A. Fadaka, B. Ajiboye, O. Ojo, O. Adewale, I. Olayide and R. Emuowhochere, *Journal of Oncological Sciences*, 2017, **3**, 45–51.
- 39 G. D. Brown, J. Bauer, H. M. Osborn and R. Kuemmerle, *ACS omega*, 2018, **3**, 17957–17975.
- 40 L. Fels and M. Bunzel, *Magnetic Resonance in Chemistry*, 2022, **60**, 692–701.